Title: The floor-plate of His is a non-neuronal electrical conduction pathway

Authors: Kalaimakan Hervé Arulkandarajah[1#], Guillaume Osterstock[1#], Agathe Lafont[1], Hervé Le Corronc[1,2], Nathalie Escalas[3], Silvia Corsini[1], Barbara Le Bras[1], Juliette Boeri[1], Antonny Czarnecki[1], Christine Mouffle[1], Erika Bullier[1], Elim Hong[1], Cathy Soula[3], Pascal Legendre[1] and Jean-Marie Mangin*[1]

# *These authors contributed equally.*

Author Affiliations:

[1]Sorbonne Université, INSERM, CNRS, Neurosciences Paris Seine - Institut de Biologie Paris Seine (NPS - IBPS), 75005 Paris, France

[2]Université d'Angers, 49000 Angers, France

[3]Centre de Biologie du Développement (CBD) CNRS/UPS, Centre de Biologie Intégrative (CBI), Université de Toulouse, Toulouse, France.

***Corresponding author:**

Jean-Marie Mangin, PhD

Laboratoire Neuroscience Paris Seine

7-9 Quai Saint Bernard

75005 Paris, France

Phone : +33 1 44 27 80 92

Email: jean-marie.mangin@inserm.fr

ABSTRACT

In the developing central nervous system of vertebrates, the emergence of electrical signals is thought to result exclusively from the differentiation of neurons[1–3]. Accordingly, the neuro-epithelial progenitors generating neurons and glial cells have been assumed to remain electrically passive. Here, we show that the floor plate of His - a neuro-epithelial organizer located at the ventral midline of the fetal spinal cord[4] - has the unexpected ability to generate large biphasic action potentials resulting from the combined activity of voltage-gated T-type calcium channels and sodium channels. Floor plate action potentials are recurrently triggered by the neurotransmitter acetylcholine released from cholinergic motor neurons during early episodes of spontaneous neural activity. Moreover, we found that floor plate cells are connected by gap junctions, form a functional syncytium with other neuro-epithelial progenitor domains and establish a ventral to dorsal depolarization gradient in the neuro-epithelium. Finally, we show that floor plate action potentials are associated with calcium waves and propagate through gap junctions along the length of the fetal spinal cord. Our present work demonstrates that the floor plate of His acts as a unique neuro-epithelial electrical conduction system, sharing functional similarities with the myo-epithelial electrical conduction system of the heart known as the bundle of His[5]. This discovery profoundly change how we conceive the development, origin, evolution and extent of electrical signals in the central nervous system of vertebrates.

MAIN TEXT

Spontaneous neural activity (SNA) plays a crucial role during the fetal development of the central nervous system of vertebrates. It has not only been shown to regulate neuronal differentiation[1–3,6], but also to influence neuro-epithelial progenitors, the stem cells of the central nervous system[7,8]. Until now, the electrical signals generated during SNA have been found to originate exclusively from differentiating neurons as they acquire the ability to fire action potentials during development. While neuro-epithelial progenitors can be depolarized by neurotransmitters released from developing neurons, they have never been reported to actively generate or propagate any form of intrinsic electrical signals[6–12].

SNA was initially described in the developing fetal spinal cord where it generates the first motor rhythmic behavior[13,14] necessary for the proper development of the neuro-muscular and musculo-skeletal systems of vertebrates[15–17]. Although the underlying molecular and cellular mechanisms have yet to be fully resolved, this initial motor program is known to rely on spontaneous waves of depolarization and electrical activity propagating in cholinergic motoneurons along the length of the developing spinal cord[17–19]. Spinal SNA is generated autonomously by the fetal spinal cord, before the establishment of sensory inputs from the periphery and descending inputs from the brain. SNA generation is therefore fully preserved in the isolated fetal spinal cord[18,19]. Neuro-epithelial progenitors in the ventral spinal cord have previously been reported to exhibit calcium transient during episodes of SNA[20], although the mechanisms remain unknown. Most neuro-epithelial calcium transients occur ventrally in the vicinity of the floor plate, a specialized neuro-epithelial structure located at the midline and spanning the entire length of the spinal cord[4,21]. The floor plate is named after the embryologist and anatomist Wilhelm His, Sr. who first identified it in 1888[21] and has since been shown to act as a major organizer for the formation of spinal motor network through the release of the morphogen Sonic Hedgehog, *Shh*[22], and the axon guidance molecules Slit and

Netrins[23]. Although the floor plate plays a central role during spinal cord development, its physiological properties remain poorly characterized.

Unlike other spinal neuro-epithelial progenitors which sequentially generate neurons and glial cells during embryonic development[24], spinal floor plate cells have only been shown to give rise to ependymocytes, a subtype of glial cells lining the central canal[25–27]. Despite this gliogenic nature, floor plate cells display T-type-like voltage-gated currents[28], suggesting that they may possess some form of electrical excitability. Therefore, to determine whether floor plate cells are able to generate intrinsic electrical signals in a physiological context, we investigated their electrophysiological properties at the onset of SNA in the spinal cord.

We first investigated whether and which T-type calcium channels are expressed in the floor plate of His around 12 days of mouse fetal development (E12), when SNA begins in the spinal cord[18,19]. By performing *in situ* hybridization against mRNA coding for the 3 known T-type calcium channels (*cacna1g*, *cacna1h, cacna1i*), we found that they were all predominantly expressed in the floor plate (**Figure 1b & 1d**). To assess their functionality, we examined the electrical properties of floor plate cells using patch-clamp recordings on a preparation of whole fetal spinal cord in the open-book configuration[19,29], giving us access to neuro-epithelial progenitors lining the central canal while preserving SNA generation (**Figure 1c)**. In the open-book configuration, floor plate cells were easily identified by their location at the midline, their thin apical processes and their higher translucency when compared to surrounding neuro-epithelial progenitor domains. To confirm the validity of these morphological criteria, some of the recorded cells were filled with the neurobiotin tracer and their molecular identity assessed by post-hoc immunostaining against the transcription factors FOXA2 and NKX2.2, which are specifically expressed in floor plate cells and in the adjacent neuro-epithelial progenitor domain known as p3, respectively[22]. All recorded cells filled by

neurobiotin were found to be FoxA2^{+} and NKX2.2^{-} (N= 10/10 cells; **Figure 1e**). At this developmental stage, all FoxA2^{+}/NKX2.2^{-} co-expressed the glutamate astrocyte transporter GLAST, a marker for glial progenitors (**Extended Data Figure 1a-h**), and the transcription factor Sox2, a marker for neuro-epithelial progenitors (**Extended Data Figure 1i-l**), confirming that the floor plate cells recorded were indeed gliogenic neuro-epithelial progenitors[30,31]. Recorded cells had an average membrane resistance of 480 ± 410 MOhms, an average membrane capacitance of 18.3 ± 6.6 pF and an average membrane potential of -64.8 ± 9.7 mV (N= 24 cells). We discovered that floor plate cells have the ability to generate action potentials (AP) in response to membrane depolarization (threshold = - 38 ± 11 mV; amplitude = 44 ± 17 mV; N= 17 cells; **Figure 1f, left trace**). Unlike neuronal APs which only rely on voltage-gated sodium channel, floor plate APs could only be fully blocked by a combination of TTA-P2 (**Figure 1f, middle trace**), a specific T-type calcium channel blocker, and TTX, a sodium channel blocker (**Figure 1f, right trace**; N = 15 cells). By contrast, neuro-epithelial progenitors recorded in the adjacent p3 domain did not exhibit any voltage-dependent potentials (N= 24 cells; **Figure 1g**). Interestingly, we found that floor plate cells spontaneously generate recurrent APs (amplitude = 54 ± 15 mV; N = 22 cells; **Figure 1h**) at an interval of 186 ± 42 s, similar to the interval previously reported in cholinergic motoneurons during spinal SNA[19]. These spontaneous events were comprised of a small initial depolarization (amplitude = 6.9 ± 1.0 mV; half-width = 2.8 ± 1.0 s) followed by an AP exhibiting a biphasic time course comprised first of a slow component (amplitude = 18.9 ± 5.5 mV; half-width = 274 ± 57 ms) followed by a fast component (amplitude = 42.4 ± 7.2 mV; half-width = 11.8 ± 3.2 ms; **Figure 1i**). Identical events could be evoked using an electrical stimulation (32 mA, 200 µs) placed on the midline, 2 mm rostrally to the site of recording (**Figure 1j**). Application of the T-type calcium channel blocker TTA-P2 (3 µM) was

sufficient to fully block the biphasic action potential, while the small initial depolarization remained unaffected (N=8/8 cells).

Since SNA is controlled by acetylcholine released from motoneurons[18,19], we investigated whether these spontaneous events could be triggered by the release of this neurotransmitter during episodes of SNA. First, we found that both spontaneous and evoked floor plate events were fully blocked by antagonists against nicotinic acetylcholine receptors (nAChRs; Mecamylamine and d-Tubocurarine; N = 12/12 cells; **Figure 2a & b**). By contrast, they remained unaffected by antagonists against $GABA_A$ receptors (Gabazine) and glutamate ionotropic receptors (DL-APV and CNQX), two other neurotransmitters released by spinal interneurons during SNA[18,19] (**Figure 2c;** N = 11/11 cells). Exogenous application of acetylcholine (30 μM) was sufficient to depolarize floor plate cells (Amplitude = 10.0 ± 1.5 mV) and trigger biphasic action potentials (amplitude = 59 ± 7 mV) in a nAChR dependent manner (N=6/6 cells) (**Figure 2d**). Application of the sodium channel blocker TTX together with antagonists of GABA, glutamate and glycine ionotropic receptors had no effect on the depolarization induced by acetylcholine, suggesting that acetylcholine acts directly onto nAChR expressed by floor plate cells (**Figure 2d)**. We observed that TTX suppressed the fast component of the biphasic action potential triggered by acetylcholine, demonstrating that it resulted from the activation of voltage-gated sodium channels in floor plate cells, while the slow component was blocked by TTA-P2 indicating that this resulted from the activation of T-type calcium channels (**Extended Data Figure 2**). To further confirm that ACh release from motoneurons triggers floor plate action potentials, we performed optogenetic stimulation of cholinergic spinal motoneurons using a transgenic mouse model (ChAT:ChR2-YFP) where channelrhodopsin 2 is expressed in cholinergic motoneurons (**Figure 2e-f**). Using this approach, we confirmed that the release of endogenous acetylcholine triggered by optogenetic stimulation of motoneurons was sufficient to depolarize and trigger an action potential in floor

plate cells (N = 9 cells), which could be fully blocked by nAChR antagonists (N = 4/4 cells; **Figure 2g)**. Taken together, our results show that floor plate action potentials are triggered by the activation of nAChR in response to acetylcholine released by motoneurons during SNA.

Unlike spinal neurons, neuro-epithelial progenitors are known to be extensively coupled by gap-junctions at this developmental stage[32]. Accordingly, neurobiotin filling of floor plate cells often labeled adjacent cells (6.6 ± 2.9 cells, N = 10), indicating gap-junction coupling (**Figure 1e**). Therefore, we investigated whether floor plate cells are electrically coupled via gap-junction with other ventral neuro-epithelial progenitor domains and whether action potentials generated in the floor plate can passively propagate into the other domains. To address this question, we performed paired recordings between floor plate cells and neuro-epithelial progenitors located in the neighboring p3 domain (Distance $_{[FP\text{-}p3]}$ = 22 ± 7 µm, N = 6; **Figure 3a-c)**. Neurobiotin filling of neuro-epithelial cells recorded in the p3 domain was found to label many adjacent cells (14.7 ± 6.3 cells, N = 6), confirming extensive gap-junction coupling (**Figure 3a)**. More importantly, spontaneous action potentials recorded in floor plate cells were found to correlate with smaller depolarizations simultaneously recorded in the p3 domain (**Figure 3b**). Current steps injected in neuro-epithelial progenitors located in the p3 domain were associated with a proportional, albeit much smaller, depolarization in the floor plate cell (Ratio $_{[FP/p3]}$ = 4.6 ± 1.7 %, N = 18), confirming that they are indeed electrically coupled (**Figure 3c**). By recording neuro-epithelial progenitors in domains located more dorsally (pMN, p0-2), we discovered that they also exhibited recurrent spontaneous depolarizations with an amplitude inversely correlated to their distance from the floor plate (**Figure 3d & e**). Taken together, our results show that floor plate action potentials triggered during SNA leads to the passive depolarization of ventral neuro-epithelial progenitors in a ventro-dorsal amplitude gradient (**Figure 3f**).

Finally, we examined whether and how floor plate activity could propagate between floor plate cells along the rostro-caudal axis of the spinal cord. To investigate this possibility, we expressed the genetically encoded calcium indicator GCaMP6f specifically in floor plate cells using a conditional transgenic approach (GCaMP6floxP x GLASTCreERT2; see Methods). This was achieved by taking advantage of the fact that floor plate cells are the first neuro-epithelial cells to express the glutamate aspartate transporter (GLAST), an early marker of gliogenesis during spinal cord development[30,31,33] (**Figure 4a** and **Extended Data Figure 1**). Using this approach, we found that midline floor plate cells expressing GCaMP6f (**Figure 4a**) generated spontaneous calcium waves at an interval of 176 ± 67 s (N = 10 embryos; **Figure 4b & c**), similar to the interval observed for spontaneous floor plate action potentials. Spontaneous floor plate calcium waves propagated along the length of the spinal cord and could propagate in either direction. However, rostral to caudal waves initiated in the cervical area were more frequent (67%, 41/61 waves, N = 10 embryos) than caudal to rostral ones (33%, 20/61 waves) **(Extended Data Figure 3** and **Extended Data video 2)**. This proportion was similar to that previously reported for waves of SNA-associated muscle contractions observed *in vivo* in mouse embryos at the same developmental stage[14]. Average propagation speed of spontaneous rostro-caudal (2.4 ± 0.9 mm/s) and caudo-rostral floor plate calcium waves (2.1 ± 1.3 mm/s) were not significantly different (paired Wilcoxon test, p=0.12, N = 10 embryos) and their speed was consistent with the propagation speed estimated for SNA waves in motoneurons[18,34].

As observed for floor plate action potentials, calcium waves could also be consistently triggered using electrical stimulation (32 mA, 200 µs, **Figure 4g, h, j, k** and **Extended Data Video 3**). Application of the T-type calcium channel blocker TTA-P2 (3 µM) was sufficient to fully block floor plate calcium waves evoked by electrical stimulation (paired Wilcoxon test, p<0.001, N = 5 embryos; **Extended Data Video 4**), even after increasing the duration of

stimulation (32 mA, 1200-1600 µs**)**. The initiation and propagation of floor plate calcium waves evoked by electrical stimulation was blocked by the application of nAChR antagonists (paired Wilcoxon test, $p<0.001$, N = 6 embryos; **Figure 4g, Extended Data video 5**), as with the floor plate action potentials (**Figure 2**). However, increasing the duration of stimulation (32 mA, 1200-1600 µs) allowed the recovery of floor plate calcium waves, albeit with a significantly decreased propagation speed of 0.8 ± 0.5 mm/s (paired Wilcoxon test, $p<0.001$, N = 6 embryos; **Figure 4g & h, Extended Data video 5**). Similarly, patch-clamp experiments showed that after increasing the duration of stimulation in the presence of a cocktail of antagonists to nAChRs, GABAaR, GluRs and GlyR, the electrical stimulus could directly trigger a delayed biphasic AP without the small initial cholinergic depolarization (N = 4 embryos; **Figure 4i**). This result shows that, although the initiation and subsequent propagation of floor plate APs and calcium waves strongly depend on cholinergic transmission from motoneurons, direct electrical coupling between floor plate cells (**Figure 1e**) also likely participates to this propagation. We tested this hypothesis by applying the gap-junction blocker β18-GA[35]. We found that it either reduced or blocked the propagation of the floor plate calcium waves (paired Wilcoxon test, $p<0.05$, N=6 embryos; **Figure 4j & k, Extended Data video 5**) and action potentials (N=4 embryos; **Figure 4l**) that were evoked in the presence of nAChR antagonists and other neurotransmitter antagonists. Therefore, these results show that the floor plate possess an intrinsic ability to both generate and propagate electrical signals along the fetal spinal cord.

To our knowledge, the floor plate of His is the first example of a non-neuronal structure able to not only generate but also propagate action potentials in the fetal central nervous system. Until now, these abilities were considered to be exclusive features of developing neurons. Accordingly, the ability to generate action potentials has been routinely

used as a functional assay to confirm the neuronal phenotype of cells during development. In this context, although Ca^{++}/Na^{+} biphasic action potentials relying on T-type calcium channels are not commonly observed in neurons, their previous discovery in neural cells in the Xenopus embryonic spinal cord[36] and in the mouse fetal hindbrain[37] has been interpreted as an early and transient form of excitability in developing neurons. Instead, we found here that Ca^{++}/Na^{+} biphasic action potentials are generated in the mouse spinal cord by gliogenic floor plate cells located at the midline and that they propagate laterally into ventral neuro-epithelial cells also engaged into a gliogenic program at this stage[30].

From an evolutionary point of view, the discovery of an epithelial electrical conduction system in the vertebrate fetal CNS should not come as a complete surprise. Indeed, epithelial and syncytial conduction systems are commonly observed in non-bilaterian animals exhibiting either a "primitive" nervous system, like jellyfish and comb jellies, or in those lacking a nervous system like the glass sponges[38–41]. It has been proposed that the modern neuron-based nervous systems of bilaterians using axonal/chemical synaptic transmission evolved from such epithelial conduction systems coupled electrically by gap-junctions[42]. This evolution would also have been accompanied by a switch from slow voltage-gated calcium channel - inherited from our protist ancestors and still found in the modern paramecium[43] - to fast voltage-gated sodium channels[42]. Our discovery of a "primitive" electrical conduction system in the neuro-epithelium that gives rise to the "modern" nervous system of vertebrates during fetal development could therefore be interpreted as strong evidence supporting this evolutionary scenario.

One may also notice the functional similitude existing between the floor plate of His and the heart electrical conduction system known as the bundle of His. The bundle of His was discovered by the anatomist and cardiologist Wilhem His, Jr. in 1893[5], five year after his father had described the floor plate[21]. Both structures act as electrical conduction systems

connected by gap junctions able to propagate electrical signals across their respective organs. By showing that these structures not only share the same name but also share similar functional properties, our work reveal that the nervous and cardiac physiology of vertebrates may be more deeply related than previously thought.

Further work will be needed to decipher what function(s) are fulfilled by this newfound non-neuronal electrical conduction system. Although the electrical excitability of floor plate cells could only be a vestigial property inherited from non-bilaterian ancestors, it is more likely playing a significant role in the development of the spinal cord. Indeed, the energetic cost of generating and propagating electrical signals[44] as well as the redundancy of T-type channel subtypes expressed in the floor plate point towards having a conserved and significant function. One hypothesis is that floor plate excitability regulates and coordinates the release of the morphogen Shh, required for neural tube patterning, or the expression of axon guidance molecules such as Slit and Netrin. Indeed, recent studies have shown unexpected interactions between early calcium electrical excitability and Sonic Hedgehog signalling in the Xenopus spinal cord[45,46]. Moreover, T-type channel mutants have recently been identified in a forward genetic screen for neural tube defects in Ciona intestinalis[47], suggesting that the electrical gradient established by the floor plate in the ventral neuro-epithelium could represent a novel morphogenetic mechanism. An additional and non-exclusive hypothesis is that floor plate action potentials initiated by acetylcholine released by motoneurons during SNA act as a feedback signal to promote the switch from neurogenesis to gliogenesis in ventral neuro-epithelial progenitors[30,31] since both events occur at the same developmental stage.

In conclusion, the discovery that the floor plate of His acts as a non-neuronal electrical conduction system profoundly change how we conceive the origin, extent and role of electrical signals during the development of the central nervous system of vertebrates.

METHODS

Mouse strains and transgenic models

All experiments were performed in accordance with European Community guiding principles on the care and use of animals (86/609/CEE, CE Off J no. L358, 18 December, 1986), French decree no. 97/748 of October 19, 1987 (J Off République Française, 20 October, 1987, pp. 12245–12248) and recommendations from the CNRS. All efforts were made to minimize the suffering of animals. In order to maximize litter size, experiments were performed on E12.5 mouse embryos obtained by crossing C57BL/6 males with females from a Swiss strain. For optogenetic stimulation of cholinergic motoneurons, we used C57BL/6 breeding male mice expressing a BAC transgene containing a Channelrhodopsin2-EYFP sequence driven by a Choline Acetyl Transferase (ChAT) promoter (ChAT-ChR2–EYFP, The Jackson Laboratory, USA, https://www.jax.org/strain/ 014546)[48]. For calcium imaging of floor plate cells, we used C57BL/6 breeding male mice expressing a genetically encoded floxed Calcium indicator GCaMP6f (Ai95, The Jackson Laboratory, USA, https://www.jax.org/strain/028865), crossed with Swiss female mice expressing a tamoxifen-inducible Cre recombinase under the control of the glutamate aspartate transporter promoter (GLASTCreERT2, gift from Dr Frank Pfrieger)[49]. Cre recombination was induced by oral gavage of pregnant mice with 5 mg of tamoxifen (Sigma-Aldrich, France, T-5648) at embryonic days E10.5 and E11.5[50]. Tamoxifen was dissolved in corn oil at 37°C for several hours to prepare 20 mg/mL solution[51].

In situ RNA hybridization staining

Mouse embryos were fixed in 3.7% paraformaldehyde (PFA) in PBS overnight at 4°C. Tissues were then sectioned at 60–80 µm using a vibratome (Microm, France). In all experiments, sections were performed at the cervico/brachial level. In situ hybridization (ISH)

was performed on vibratome sections automatically (InsituPro, Intavis, Germany) using the whole-mount ISH as previously reported[52]. Digoxigenin (DIG)-labeled antisense RNA probes were synthesized using T3 polymerase from the following I.M.A.G.E. Consortium cDNA Clones[53]: *cacna1g*, (ID 6410519); *cacna1h* (ID 6820407) and *cacna1i* (ID 6825802). RNA labeled probes were detected by an alkaline-phosphatase coupled antibody (Roche Diagnostics), and NBT/BCIP (nitroblue tetrazolium/5-bromo-4-chloro-3-indolyl phosphate) were used as a chromogenic substrate for the alkaline phosphatase (Boehringer Mannheim, Germany). Stained sections were digitized and analyzed using Zeiss acquisition software (Zeiss, Germany).

Isolated embryonic spinal cord preparation

E12.5 embryonic mouse spinal cords were dissected as previously described[19,29]. Briefly, pregnant mice were killed using a lethal dose of CO_2 followed by cervical dislocation. Mice embryos of both sexes were dissected and whole spinal cord were left to recover for at least 30 min at 32˚C in artificial cerebrospinal fluid (ACSF) containing 125 mM NaCl, 25mM NaHCO3, 11 mM Glucose, 3 mM KCl, 1 mM MgCl2, 2 mM CaCl2, and 1 mM NaH2PO4 (pH 7.3; 307 mOsm) continuously bubbled with 95% O_2 – 5% CO_2 gas, before being recorded or imaged. For ChAT-ChR2-EYFP and GCaMP6floxP x GLASTCreERT2 transgenic embryos, their tails were cut and observed under a fluorescent stereo-microscope (Leica MZ FLIII) to identify positive embryos for EYFP and GCaMP6, respectively.

Patch-clamp recordings

Isolated spinal cords were placed in open-book configuration in a recording chamber under a nylon holding grid and continuously perfused (2 ml/min) at room temperature with the oxygenated ACSF described above. In contrast to previous studies[19,29], the orientation of

open-book spinal cord was inverted so that the neuro-epithelial layer was facing upward. Whole-cell voltage-clamp recordings of floor plate cells and other neuroepithelial progenitors were performed under direct visualization using an infrared-sensitive CCD video camera. In addition to their location at the midline, floor plate cells were distinguished from surrounding neuro-epithelial progenitors based on their smaller apical process and their higher translucency when using brightfield microscopy. To confirm their identity, some recorded cells were filled with neurobiotin (1 mg/ml, Vector labs) and revealed in combination with FoxA2 and Nkx2.2 immunostaining. Whole-cell patch-clamp electrodes were pulled from thick-wall borosilicate glass using a Brown-Flaming puller (P97, Sutter Instrument, USA). The tip of the electrode was fire-polished using a microforge (MF-830, Narishige, Japan). Patch-clamp electrodes had tip resistances comprised between 4 and 7 MΩ. Electrodes were filled with an intracellular solution containing either (in mM): 96.4 K^+-methanesulfonate, 33.6 KCl, 4 MgCl2, 4 Na_2ATP, 0.3 Na_3GTP, 10 EGTA, and 10 HEPES or 100 K^+-gluconate, 34 KCl, 0.5 EGTA, 10 HEPES, 4 $MgCl_2$, 4 Na_2ATP (pH 7.2; 290 mOsm). In both solutions, the theoretical equilibrium potential for chloride ions (ECl) was -30 mV, while cation reversal potential (Ecat) was 0 mV. Signals were recorded with a low-pass filtered at 4 kHz using a Multiclamp 700B amplifier (Molecular Devices, San Jose, CA, USA) and digitized at 20 kHz using a Digi-data 1440A interface coupled to pClamp 10.5 software (Molecular Devices, San Jose, CA, USA) running on a PC computer. Cells exhibiting a resting membrane potential above -50 mV (I=0 pA) were discarded from further analysis.

Electrical and optogenetic stimulation

For electrical stimulations experiments, we used bipolar platinum electrodes (FHC, Bowdoin, ME, USA) placed 2 mm rostrally to the recording site onto the midline. For optogenetic stimulation of ChAT-ChR2 we used a 400 µm diameter optical fiber coupled with

a 470 LED (Thorlabs, Germany) and centered onto the recording site. Electrical and optogenetic stimulations were performed at a low frequency (0.005 Hz, 1 stimulation every 180 s) in order to evoke a stable cholinergic response.

Calcium imaging

Isolated spinal cords were placed in open-book configuration under a nylon holding grid in a recording chamber and continuously perfused (2mL/min) with the same oxygenated ACSF described above. Recombined fluorescent cells were observed under an epifluorescence microscope BX51W1 (Olympus) with a 470-515nm fluorescent excitation light to confirm GCaMP6f expression in the floor plate. Time-lapse imaging was performed using either an Orca Flash4.0 (Hamamatsu, Japan) or Orca 03G (Hamamatsu, Japan) camera and recorded using the HC Image Live software (Hamamatsu, Japan) at an acquisition frequency of 5 or 10Hz with an exposure time of 200 ms and 100 ms, respectively. Images were encoded using a 256x256 or 512x512 pixel resolution and 16-bit grey scale. Time-lapse images were analyzed using the ImageJ software (National Institute of Health, USA). Signals were either extracted by subtracting each frame from the one following it (Figure 4g & 4i) or by subtracting an average of 10 frames preceding the onset of an event (Figure 4d, Extended Data Figure 3 and Extended Data videos 1-5). To measure the propagation speed, we pinpointed three regions of interest on the midline and measured the delays necessary to reach half-peak between each region of interest and averaged them. Intensity of signals (dF/F) were measured by dividing the peak amplitude of the events by the baseline value in raw images.

Pharmacological agents

In most experiments, drugs were applied via the bath perfusion system. Typically, the effect of drugs reached equilibrium within 3 to 5 minutes. For acetylcholine application, we

used a 0.5 mm diameter quartz tubing positioned 50 µm away from the recording area under direct visual control. Typically, response to acetylcholine reached equilibrium a few seconds (6 sec) after solution switch. The quartz tubing was connected using a manifold to six solenoid valves linked with six reservoirs. Solutions were gravity-fed into the quartz tubing. Drug application was controlled using a VC-8 valve controller (Warner Instruments, USA). At least 3 events were recorded in each condition after waiting 5 min for drugs to act. The following pharmacological agents were used: Acetylcholine chloride (30 µM, Sigma-Aldrich, Germany), TTX (1 µM, Alomone Labs, Israel), gabazine (3 µM, Tocris, USA), CNQX Disodium (20 µM, Tocris, USA), DL-APV (200 µM, Tocris, USA), Mecamylamine hydrochloride (100 µM, Tocris, USA), D-turbocurarine chloride (10 µM,Tocris Bioscience, Minneapolis, MN, USA), 18- β glycyrrhetinic acid (50 µM, Sigma-Aldrich, Germany) and TTA-P2 (3µM, Alomone, Israel). All drugs were dissolved at final concentration in ACSF.

Immunohistochemistry

E12.5 embryos or whole embryonic spinal cord were immersion-fixed in phosphate buffer saline (PBS) with 4% PFA freshly prepared in PBS (pH 7.4) for 1 h at 4°C. Embryos were then rinsed with PBS and cryoprotected in PBS-15% sucrose at 4°C for 24 h and then in PBS-30% sucrose at 4°C for 24 h. Embryos were embedded in OCT medium (VWR, USA) and quickly frozen. Serial sections 20 µm thick were collected onto slides using a cryostat (Leica, Wetzlar, Germany) and stored at -80°C until immunohistochemical studies. For immunostaining, slides and whole spinal cord were washed in PBS, incubated in NH_4Cl (50 mM) diluted in PBS for 20 min and then permeabilized for 30 min in a blocking solution (10% goat serum in PBS) with 0.2% Triton X-100. They were incubated overnight at 4°C with the primary antibodies, which were diluted in the 0.2% Triton X-100 blocking solution. Slides or whole spinal cords were then washed in PBS and incubated for 2h at room

temperature in the appropriate secondary antibodies (diluted at 1/1000 in the 0.2% Triton X-100 blocking solution). The following primary antibodies were used: a mouse monoclonal anti-HNF-3β/FoxA2 (H-4) antibody sc-374376 (1:300, Santa Cruz Biotechnology, USA), a mouse monoclonal anti-Nkx2.2 antibody 74.5.A5 (1:600, Developmental Studies Hybridoma Bank, USA), a guinea-pig polyclonal anti-EAAT1/GLAST antibody 250 114 (1:1000, Synaptic System, Germany), a rabbit polyclonal anti-VAChT antibody (1:1000, Synaptic System, Germany) and a rabbit polyclonal anti-GFP antibody (1:1000, Invitrogen, USA). Alexa Fluor 405-, 488-, or 594- and 647-conjugated secondary antibodies (1/1000; Invitrogen, USA) were used to detect mouse monoclonal, guinea pig and rabbit polyclonal primary antibodies. After washing in PBS, slides or whole spinal cords were dried and mounted in Mowiol medium (Millipore, USA).

Confocal microscopy

Once mounted, immunostained sections were imaged using a SP5 confocal microscope (Leica, Germany) using a 20X oil-immersion objective with a numerical aperture of 1.25, as well as with a 63X oil-immersion objective with a numerical aperture of 1.32 and a 1X digital zoom magnification. Serial optical sections were acquired with a Z-step of 3 µm (20X) and 0.78 µm (63X). Images (1024 X 1024; 8 to16 bit grayscale) were acquired using Leica software LAS-AF and analyzed using ImageJ (National Institutes of Health, USA). Colocalization with neurobiotin staining was assessed in three axes using a single confocal slice and x and y orthogonal views of the stack (ImageJ 1.5).

Statistics

Statistical comparisons for electrophysiological recordings and calcium imaging parameters were conducted using GraphPad Prism 8 by performing non-parametric Wilcoxon-Mann-

Whitney U tests for independent samples and Wilcoxon signed rank test for paired samples. We determined that statistical significance was obtained when the two-tailed p-value was <0.05.

DATA AVAILABILITY

The authors declare that the data supporting the findings of this study are available within the paper.

REFERENCES

1. Moody, W. J. & Bosma, M. M. Ion channel development, spontaneous activity, and activity-dependent development in nerve and muscle cells. *Physiological Reviews* vol. 85 883–941 (2005).

2. Spitzer, N. C. Electrical activity in early neuronal development. *Nature* vol. 444 707–712 (2006).

3. Blankenship, A. G. & Feller, M. B. Mechanisms underlying spontaneous patterned activity in developing neural circuits. *Nature Reviews Neuroscience* vol. 11 18–29 (2010).

4. Placzek, M. & Briscoe, J. The floor plate: Multiple cells, multiple signals. *Nature Reviews Neuroscience* vol. 6 230–240 (2005).

5. BAST, T. H. & GARDNER, W. D. Wilhelm His, Jr. and the Bundle of His. *J. Hist. Med. Allied Sci.* **IV**, 170–187 (1949).

6. Kirischuk, S. *et al.* Modulation of neocortical development by early neuronal activity: Physiology and pathophysiology. *Frontiers in Cellular Neuroscience* vol. 11 (2017).

7. LoTurco, J. J., Owens, D. F., Heath, M. J. S., Davis, M. B. E. & Kriegstein, A. R. GABA and glutamate depolarize cortical progenitor cells and inhibit DNA synthesis. *Neuron* **15**, 1287–1298 (1995).

8. Weissman, T. A., Riquelme, P. A., Ivic, L., Flint, A. C. & Kriegstein, A. R. Calcium waves propagate through radial glial cells and modulate proliferation in the developing neocortex. *Neuron* **43**, 647–661 (2004).

9. Corlew, R., Bosma, M. M. & Moody, W. J. Spontaneous, synchronous electrical activity in neonatal mouse cortical neurones. *J. Physiol.* **560**, 377–390 (2004).

10. Vitali, I. *et al.* Progenitor Hyperpolarization Regulates the Sequential Generation of Neuronal Subtypes in the Developing Neocortex. *Cell* **174**, 1264-1276.e15 (2018).

11. Noctor, S. C. *et al.* Dividing precursor cells of the embryonic cortical ventricular zone have morphological and molecular characteristics of radial glia. *J. Neurosci.* **22**, 3161–3173 (2002).

12. Rosa, J. M. *et al.* Neuron-glia signaling in developing retina mediated by neurotransmitter spillover. *Elife* **4**, (2015).

13. Hamburger, V. & Balaban, M. Observations and experiments on spontaneous rhythmical behavior in the chick embryo. *Dev. Biol.* **7**, 533–545 (1963).

14. Suzue, T. & Shinoda, Y. Highly reproducible spatiotemporal patterns of mammalian embryonic movements at the developmental stage of the earliest spontaneous motility. *Eur. J. Neurosci.* **11**, 2697–2710 (1999).

15. Landmesser, L. T. General principles of spinal motor circuit development: early contributions from research on avian embryos. *Int. J. Dev. Biol.* **62**, 235–243 (2018).

16. Shwartz, Y., Blitz, E. & Zelzer, E. One load to rule them all: Mechanical control of the musculoskeletal system in development and aging. *Differentiation* **86**, 104–111 (2013).

17. Hanson, M. G., Milner, L. D. & Landmesser, L. T. Spontaneous rhythmic activity in early chick spinal cord influences distinct motor axon pathfinding decisions. *Brain Res. Rev.* **57**, 77–85 (2008).

18. Hanson, M. G. & Landmesser, L. T. Characterization of the circuits that generate spontaneous episodes of activity in the early embryonic mouse spinal cord. *J. Neurosci.* **23**, 587–600 (2003).

19. Czarnecki, A. *et al.* Acetylcholine controls GABA-, glutamate-, and glycine- dependent giant depolarizing potentials that govern spontaneous motoneuron activity at the onset of synaptogenesis in the mouse embryonic spinal cord. *J. Neurosci.* **34**, (2014).

20. Wang, S., Polo-Parada, L. & Landmesser, L. T. Characterization of Rhythmic Ca2+ Transients in Early Embryonic Chick Motoneurons: Ca2+ Sources and Effects of Altered Activation of Transmitter Receptors. *J. Neurosci.* **29**, 15232–15244 (2009).

21. Kingsbury, B. F. The extent of the floor-plate of his and its significance. *J. Comp. Neurol.* **32**, 113–135 (1920).

22. Lupo, G., Harris, W. A. & Lewis, K. E. Mechanisms of ventral patterning in the vertebrate nervous system. *Nature Reviews Neuroscience* vol. 7 103–114 (2006).

23. Chédotal, A. Roles of axon guidance molecules in neuronal wiring in the developing spinal cord. *Nature Reviews Neuroscience* vol. 20 380–396 (2019).

24. Rowitch, D. H. Glial specification in the vertebrate neural tube. *Nat. Rev. Neurosci.* **5**, 409–19 (2004).

25. Mirzadeh, Z. *et al.* Bi- and uniciliated ependymal cells define continuous floor-plate-derived tanycytic territories. *Nat. Commun.* **8**, (2017).

26. Khazanov, S. *et al.* Floor plate descendants in the ependyma of the adult mouse Central Nervous System. *Int. J. Dev. Biol.* **61**, 257–265 (2017).

27. Cañizares, M. A. *et al.* Multiple steps characterise ventricular layer attrition to form the ependymal cell lining of the adult mouse spinal cord central canal. *J. Anat.* (2019) doi:10.1111/joa.13094.

28. Frischknecht, F. & Randall, A. D. Voltage- and ligand-gated ion channels in floor plate neuroepithelia of the rat. *Neuroscience* **85**, 1135–49 (1998).

29. Osterstock, G. *et al.* Axoglial synapses are formed onto pioneer oligodendrocyte precursor cells at the onset of spinal cord gliogenesis. *Glia* (2018) doi:10.1002/glia.23331.

30. Deneen, B. *et al.* The Transcription Factor NFIA Controls the Onset of Gliogenesis in the Developing Spinal Cord. *Neuron* **52**, 953–968 (2006).

31. Barry, D. & McDermott, H. Differentiation of radial glia from radial precursor cells and transformation into astrocytes in the developing rat spinal cord. *Glia* **50**, 187–197 (2005).

32. Bittman, K. S., Panzer, J. A. & Balice-Gordon, R. J. Patterns of cell-cell coupling in embryonic spinal cord studied via ballistic delivery of gap-junction-permeable dyes. *J. Comp. Neurol.* **477**, 273–285 (2004).

33. Shibata, T. *et al.* Glutamate transporter GLAST is expressed in the radial glia-astrocyte lineage of developing mouse spinal cord. *J. Neurosci.* **17**, 9212–9 (1997).

34. Scain, A.-L. *et al.* Glycine release from radial cells modulates the spontaneous activity and its propagation during early spinal cord development. *J. Neurosci.* **30**, 390–403 (2010).

35. Rozental, R., Srinivas, M. & Spray, D. C. How to close a gap junction channel. Efficacies and potencies of uncoupling agents. *Methods Mol. Biol.* **154**, 447–476 (2001).

36. Gu, X., Olson, E. C. & Spitzer, N. C. Spontaneous neuronal calcium spikes and waves during early differentiation. *J. Neurosci.* **14**, 6325–6335 (1994).

37. Moruzzi, A. M., Abedini, N. C., Hansen, M. A., Olson, J. E. & Bosma, M. M. Differential expression of membrane conductances underlies spontaneous event initiation by rostral midline neurons in the embryonic mouse hindbrain. *J. Physiol.* **587**, 5081–93 (2009).

38. Meech, R. W. Electrogenesis in the lower Metazoa and implications for neuronal integration. *Journal of Experimental Biology* vol. 218 537–550 (2015).

39. Mackie, G. O. Neuroid conduction and the evolution of conducting tissues. *The Quarterly review of biology* vol. 45 319–332 (1970).

40. Anderson, P. A. V. Epithelial conduction: Its properties and functions. *Progress in Neurobiology* vol. 15 161–203 (1980).

41. Leys, S. P., Mackie, G. O. & Reiswig, H. M. The Biology of Glass Sponges. *Advances in Marine Biology* vol. 52 1–145 (2007).

42. Castelfranco, A. M. & Hartline, D. K. Evolution of rapid nerve conduction. *Brain Res.* **1641**, 11–33 (2016).

43. Eckert, R., Naitoh, Y. & Friedman, K. Sensory mechanisms in Paramecium. I. Two components of the electric response to mechanical stimulation of the anterior surface. *J. Exp. Biol.* **56**, 683–694 (1972).

44. Attwell, D. & Laughlin, S. B. An energy budget for signaling in the grey matter of the brain. *Journal of Cerebral Blood Flow and Metabolism* vol. 21 1133–1145 (2001).

45. Belgacem, Y. H., Borodinsky, L. N. & Stevens, C. F. Inversion of Sonic hedgehog action on its canonical pathway by electrical activity. *Proc. Natl. Acad. Sci. U. S. A.* **112**, 4140–4145 (2015).

46. Borodinsky, L. N. & Belgacem, Y. H. Crosstalk among electrical activity, trophic factors and morphogenetic proteins in the regulation of neurotransmitter phenotype specification. *J. Chem. Neuroanat.* **73**, 3–8 (2016).

47. Abdul-Wajid, S., Morales-Diaz, H., Khairallah, S. M. & Smith, W. C. T-type Calcium Channel Regulation of Neural Tube Closure and EphrinA/EPHA Expression. *Cell Rep.* **13**, 829–839 (2015).

48. Zhao, S. *et al.* Cell type-specific channelrhodopsin-2 transgenic mice for optogenetic dissection of neural circuitry function. *Nat. Methods* **8**, 745–755 (2011).

49. Slezak, M. *et al.* Transgenic mice for conditional gene manipulation in astroglial cells. *Glia* **55**, 1565–1576 (2007).

50. Eon, J. P. *et al.* System for tamoxifen-inducible expression of Cre-recombinase from the Foxa2 locus in mice. *Dev. Dyn.* **237**, 447–453 (2008).

51. Zervas, M., Millet, S., Ahn, S. & Joyner, A. L. Cell behaviors and genetic lineages of the mesencephalon and rhombomere 1. *Neuron* **43**, 345–357 (2004).

52. Touahri, Y. *et al.* Sulfatase 1 promotes the motor neuron-to-oligodendrocyte fate switch by activating Shh signaling in Olig2 progenitors of the embryonic ventral spinal cord. *J. Neurosci.* **32**, 18018–18034 (2012).

53. Lennon, G., Auffray, C., Polymeropoulos, M. & Soares, M. B. The I.M.A.G.E consortium: An integrated molecular analysis of genomes and their expression. *Genomics* vol. 33 151–152 (1996).

ACKNOWLEDGEMENTS

We thank Isabelle Dusart, Marine Robouam, Odile Favière, Goran Fort and Maryse Dardenne for their help in managing mouse colonies; Susanne Bolte, Jean-François Gilles and France Lam for assistance with confocal imaging. We thank Frank Pfrieger for the GLASTCreERT2 mouse line. This study was financially supported by Institut de Recherche sur la Moelle et l'encéphale (JMM), AFM-Telethon (JMM), Agence Nationale de la Recherche (JMM) and Fondation pour la Recherche Médicale (JMM and PL).

AUTHOR CONTRIBUTIONS

K.H. Arulkandarajah, G. Osterstock and H. Le Corronc designed, performed and analysed the electrophysiological recordings. K.H. Arulkandarajah, G. Osterstock, S. Corsini and B. Le Bras designed, performed and analysed the immunohistochemistry experiments. A. Lafont, K.H. Arulkandarajah and E. Hong designed, performed and analysed calcium imaging experiments. K.H. Arulkandarajah, J. Boeri and A. Czarnecki designed, performed and analysed optogenetic experiments. N. Escalas, C. Soula, K.H. Arulkandarajah and E. Hong designed, performed and analysed *in situ* hybridization experiments. C. Mouffle and E. Bullier managed the animal colony, performed animal genotyping and contributed to immunohistochemistry experiments. J-M Mangin participated to the design and analysis of

the experiments, supervised the project and wrote the manuscript with P. Legendre, C. Soula and E. Hong.

ETHICS DECLARATIONS

Competing interests

The authors declare no competing interests.

FIGURES

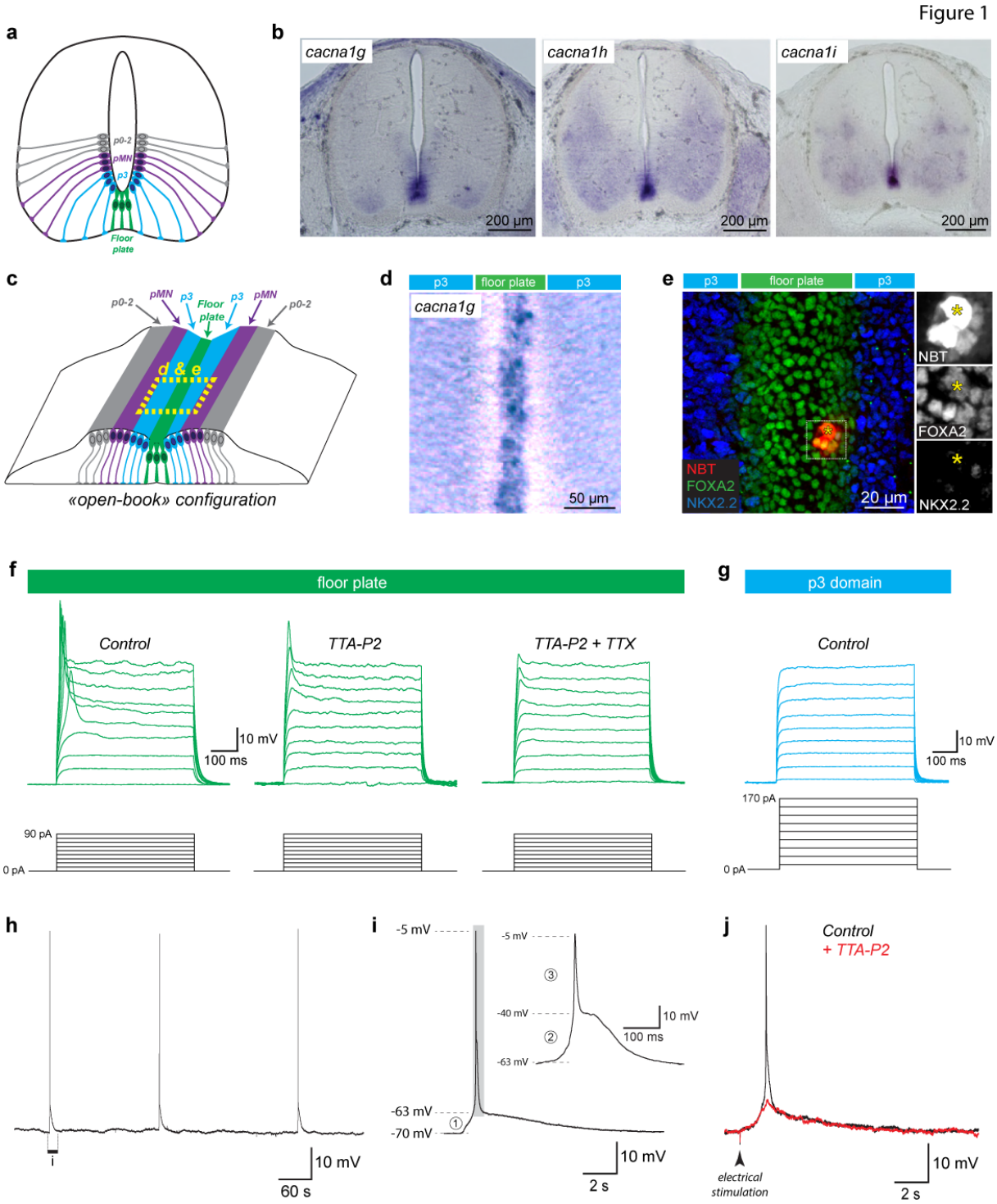

Figure 1. Floor plate neuro-epithelial progenitors express functional voltage-gated T-type calcium channels and generate recurrent action potentials during spinal SNA.
a, Drawing showing the location and radial organization of the floor plate and ventral neuro-epithelial progenitor domains (p3, pMN, p2-p0) in a coronal section of an E12.5 mouse spinal cord. **b,** *In situ* hybridization showing the location of mRNA transcripts for the 3 known sub-types of T-type channels (*cacna1g, cacna1h, cacna1i*) in coronal sections of E12.5 mouse embryos. Note that transcripts for all 3 subunits were highly expressed in the floor plate. **c,**

Drawing showing the location of the floor plate and ventral neuro-epithelial progenitor domains in the open-book configuration used for patch-clamp recordings and calcium imaging. **d,** *In situ* hybridization showing location of mRNA transcripts for *cacna1g* in an E12.5 spinal cord in open-book configuration. **e,** Confocal image from an E12.5 spinal cord in open-book configuration after patch-clamp recording of a floor plate cell. The recorded floor plate cell (yellow asterisk) was filled with neurobiotin (NBT, red) and the spinal cord was processed for immunostaining against the transcription factor FoxA2 (green), expressed in floor plate cells and against the transcription factor NKX2.2 (blue) expressed in neuro-epithelial progenitors in the adjacent p3 domain. Note that several cells were filled by neurobiotin, indicating gap junction coupling between floor plate cells. **f,** Example of current-clamp recordings obtained in a floor plate cells in response to 10 incremental current steps (increment = 10pA) in control conditions (left traces), after application of the T-type calcium channel blocker TTA-P2 (3 µM; center traces) and subsequent addition of the sodium channel blocker TTX (1 µM; right traces). Note that action potentials triggered in floor plate cells were only fully blocked by a combination of both channel blockers. **g,** Example of current-clamp recordings obtained in neuro-epithelial progenitors located in the adjacent p3 domain in response to incremental current steps (increment = 20pA). Note that neuro-epithelial progenitors in the p3 domain were electrically passive in response to membrane depolarizing **h,** Example of current-clamp recording from a floor plate cell spontaneously generating recurrent action potential at the same frequency as spinal SNA. **i,** Magnified view of a spontaneous depolarization revealing the presence of three distinct components: a small initial depolarization (1, from -70 to -63 mV) and a biphasic action potential (grey area magnified in insert) composed of a slow (2, from -63 to -40 mV) and fast component (3, from -40 to -5 mV). **j,** depolarization with a time course identical to spontaneous events could also be evoked by an electrical stimulation located 3 mm rostrally to the site of recording. Application of TTA-P2 (3 µM) fully blocked the biphasic action potential while the small initial depolarization remained unaffected.

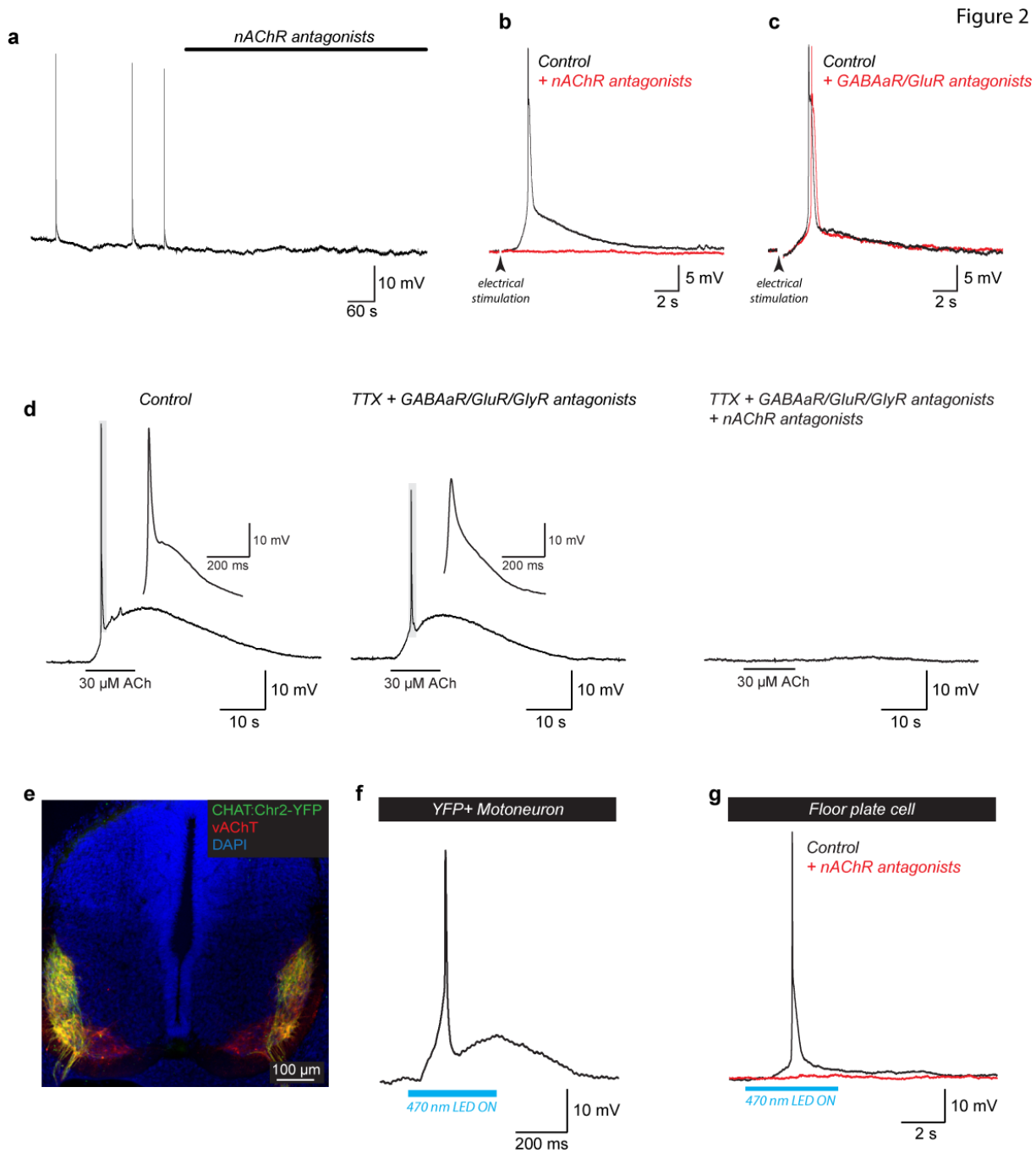

Figure 2. Floor plate biphasic action potentials are triggered by the activation of nicotinic acetylcholine receptors in response to acetylcholine released by motoneurons. **a,** Example of recurrent spontaneous floor plate action potentials blocked after addition of the nicotinic acetylcholine receptor (nAChR) antagonists: Mecamylamine (50 µM) and d-Tubocurarine (5 µM). **b,** Example of current-clamp recording showing floor plate action potential evoked by electrical stimulation in control condition (black trace) and after addition of the nAChR antagonists (red trace). **c,** Example of current-clamp recording showing floor plate action potential evoked in control condition (black trace) and after addition of antagonists against ionotropic receptor for GABA (Gabazine 3 µM) and glutamate (DL-APV 200 µM and CNQX 20 µM). **d,** Example of current-clamp recording showing that floor plate action potential can be evoked by local application of 30 µM acetylcholine (left trace), even in the presence of TTX (1 µM) and antagonists to AMPA/Kainate glutamate receptor (CNQX 10 µM), NMDA glutamate receptor (DL-APV 200 µM), $GABA_A$ receptor (Gabazine 3 µM) and

glycine receptor (strychnine 1 μM) (center trace). Floor plate action potential evoked by acetylcholine were blocked by the addition of nAChR antagonists (right trace). Note that the addition of TTX inhibited the fast component of the biphasic action potential (see **Extended Data Figure 2**). **e,** Confocal image of a coronal section from a ChAT:ChR2-YFP mouse embryo at E12.5 showing the expression of Channelrhodopsin2-YFP fusion protein (in green) in cholinergic motoneurons located in the ventro-dorsal horns and labelled with the vesicular acetylcholine transporter VAChT (in red). All cell nuclei were labelled using DAPI (in blue). **f,** Example of current-clamp recording from a ChAT:ChR2-YFP$^+$ motoneuron showing an action potential triggered by the opening of Channelrhodopsin 2 in response to blue light stimulation (470 nm). **g,** Example of current-clamp recording from a floor plate cell recorded in a ChAT:ChR2-YFP$^+$ fetal spinal cord showing how blue light stimulation could evoke a slow cholinergic depolarization and trigger a biphasic action potential that were blocked by the addition of nAChR antagonists.

Figure 3

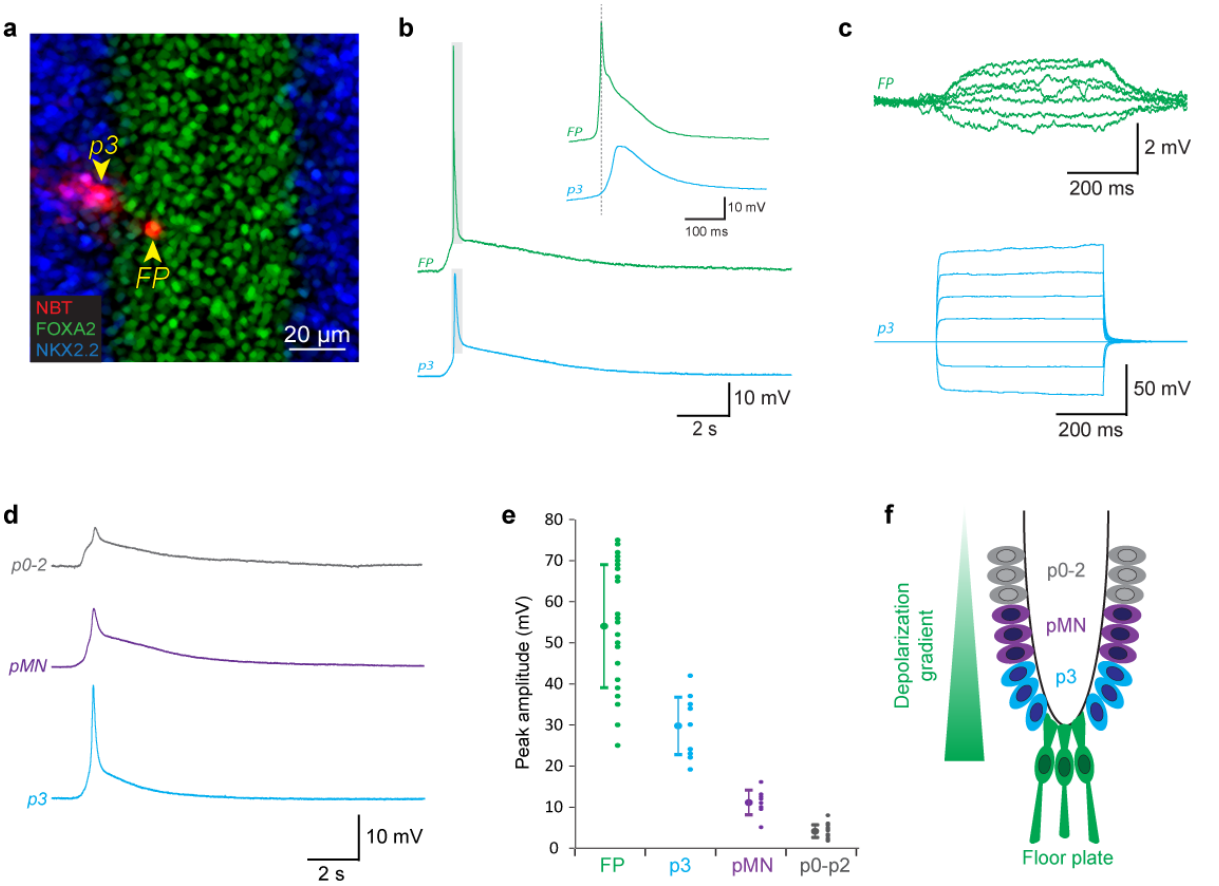

Figure 3. Floor plate action potential establishes a ventro-dorsal gradient of depolarization in the ventral neuro-epithelium.

a, Confocal image showing a pair of floor plate and p3 neuro-epithelial progenitors simultaneously recorded by dual patch-clamp and filled with neurobiotin (NBT, red). The recorded open-book preparation was processed for immunostaining against the transcription factor FoxA2 (Floor plate marker, green) and NKX2.2 (p3 domain marker, blue). The two recorded cells are indicated by yellow arrowheads. **b,** Example of a spontaneous depolarization and floor plate action potential simultaneously recorded in a floor plate and a p3 neuro-epithelial progenitor. Note the reduced amplitude and slight delay of the p3 depolarization that is consistent with passive propagation of the action potential from the floor plate to the p3 domain through gap junctions. **c,** Injection of a depolarizing current in a p3 neuro-epithelial progenitor resulted in the simultaneous depolarization of floor plate cell, confirming the existence of functional gap junctions between these cells. **d,** Example of current-clamp recording showing different spontaneous depolarizations recorded separately in neuro-epithelial progenitors from the p0-p2 domain (top trace, in grey), the pMN domain (middle trace, purple) and the p3 domain (bottom trace, blue). Domains were determined by their distance from the midline in open-book configuration (p3 = 30-70 µm; pMN = 70-110 µm; p0-p2 = 110-200). **e,** Plot showing the average amplitude and amplitude distribution of spontaneous events recorded in floor plate cells and neuro-epithelial progenitors from the 3 ventral domains. Note that amplitudes are inversely correlated to the distance of the recorded domain from the midline. **f,** Drawing illustrating the depolarization gradient observed in the ventral neuro-epithelium.

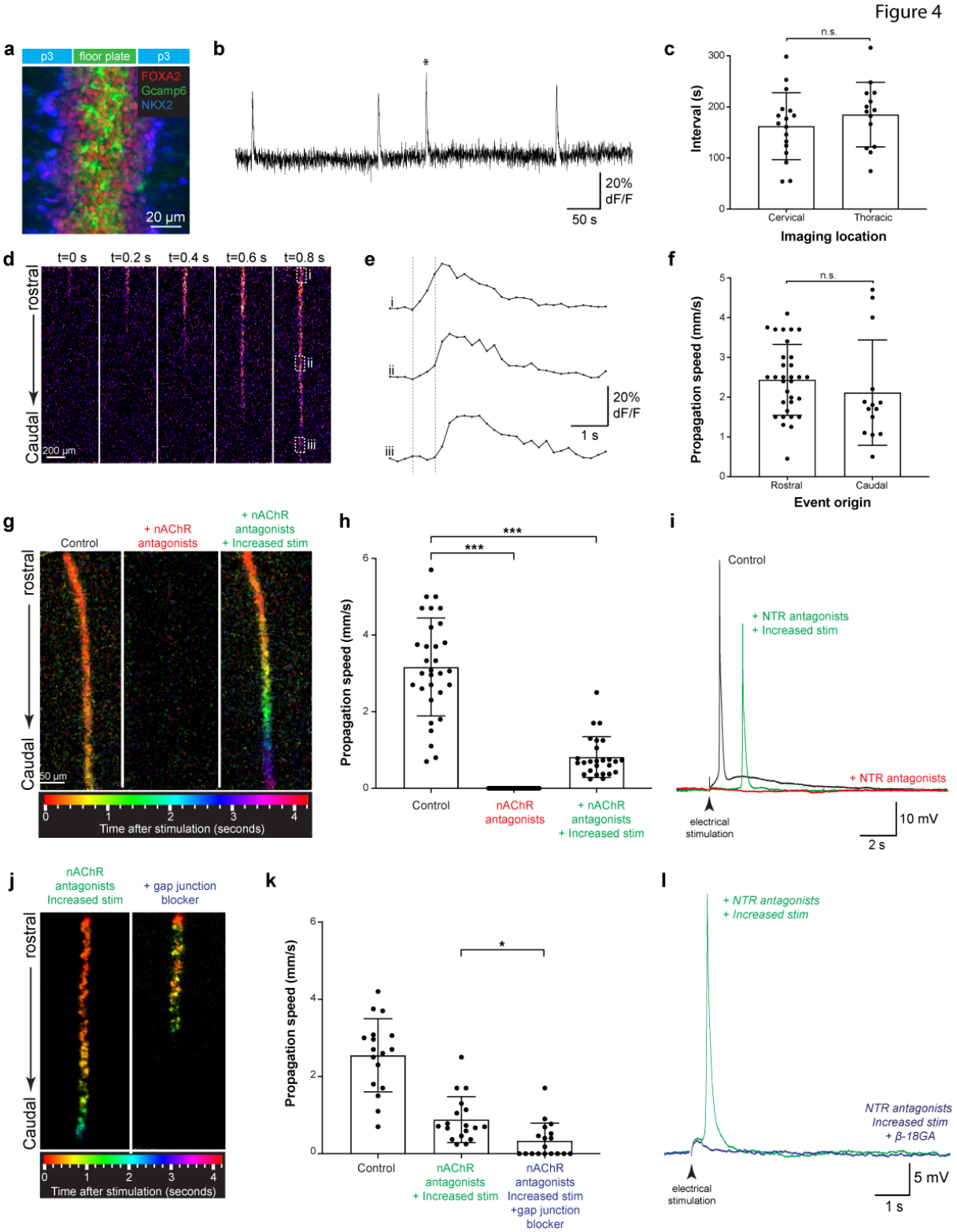

Figure 4. Floor plate action potentials are associated with calcium waves and propagate along the length of the spinal cord.

a, Confocal image showing the expression of the fluorescent GCaMP6 protein (in green) in floor plate cells labelled with an antibody against FoxA2 (in red). Recombination of GCaMP6 was not induced in the p3 domain labelled with an antibody against NKX2.2 (in blue). **b,** Plot representing the intensity of fluorescence (dF/F) in the floor plate over 10 min. Recurrent spontaneous calcium events were observed. Asterisk indicates the event represented in **d**. **c,**

Plot quantifying the interval separating spontaneous calcium events observed at cervical and thoracic segments. **d,** Time-lapse images showing the rostro-caudal propagation of GCaMP6 fluorescent signals in floor plate cells over time in the thoracic region. Dotted boxes represent the region of interest used to calculate propagation speeds. **e**, Plot representing the intensity of fluorescence (dF/F) over time in the 3 regions of interest indicated in **d**. Dotted lines mark the onset of the calcium signals in region i and iii, respectively. **f,** Plot of the propagation speed of floor plate calcium waves according to the rostral or the caudal origin of the waves (N=61 waves; 10 embryos). No significant differences in propagation speed were observed between rostral and caudal origin. **g**, Images of color-coded calcium waves evoked by rostral electrical stimulation (32 mA, 200 µs) in control condition (left), after application of nAChR antagonists (center) and subsequent increase of stimulation intensity (32 mA, 1200 µs). Time after stimulation is coded in distinct color as indicated in the scale at the bottom. Note that calcium waves evoked at higher stimulation intensity in the presence of nAChR antagonists propagate more slowly. **h**, Plots of the propagation speed of evoked floor plate calcium waves in different conditions. **i,** Example of current-clamp recording of a floor plate cell in control condition (black trace), after application of a cocktail of antagonist to nAChR, $GABA_AR$, iGluR and GlyR (red trace) and subsequent increase of stimulation intensity. Note that action potential could still be evoked and propagate even when nAChRs, $GABA_ARs$, iGluRs and GlyRs were blocked. **j,** Images of color-coded calcium waves evoked by increased electrical stimulation (32 mA, 1200 µs) in the presence of nAChR antagonists (left panel) and after addition of the gap junction blocker β18-GA (right panel). **k**, Plot of the propagation speed of evoked floor plate calcium waves before and after addition of nAChR antagonists and gap junction blockers. **l**, Example of current-clamp recording of a floor plate cell in the presence of a cocktail of antagonists to nAChR, $GABA_AR$, iGluR and GlyR (green trace) and after subsequent addition of the gap junction blocker β18-GA (blue trace).

EXTENDED DATA FIGURES

Extended Data Figure 1

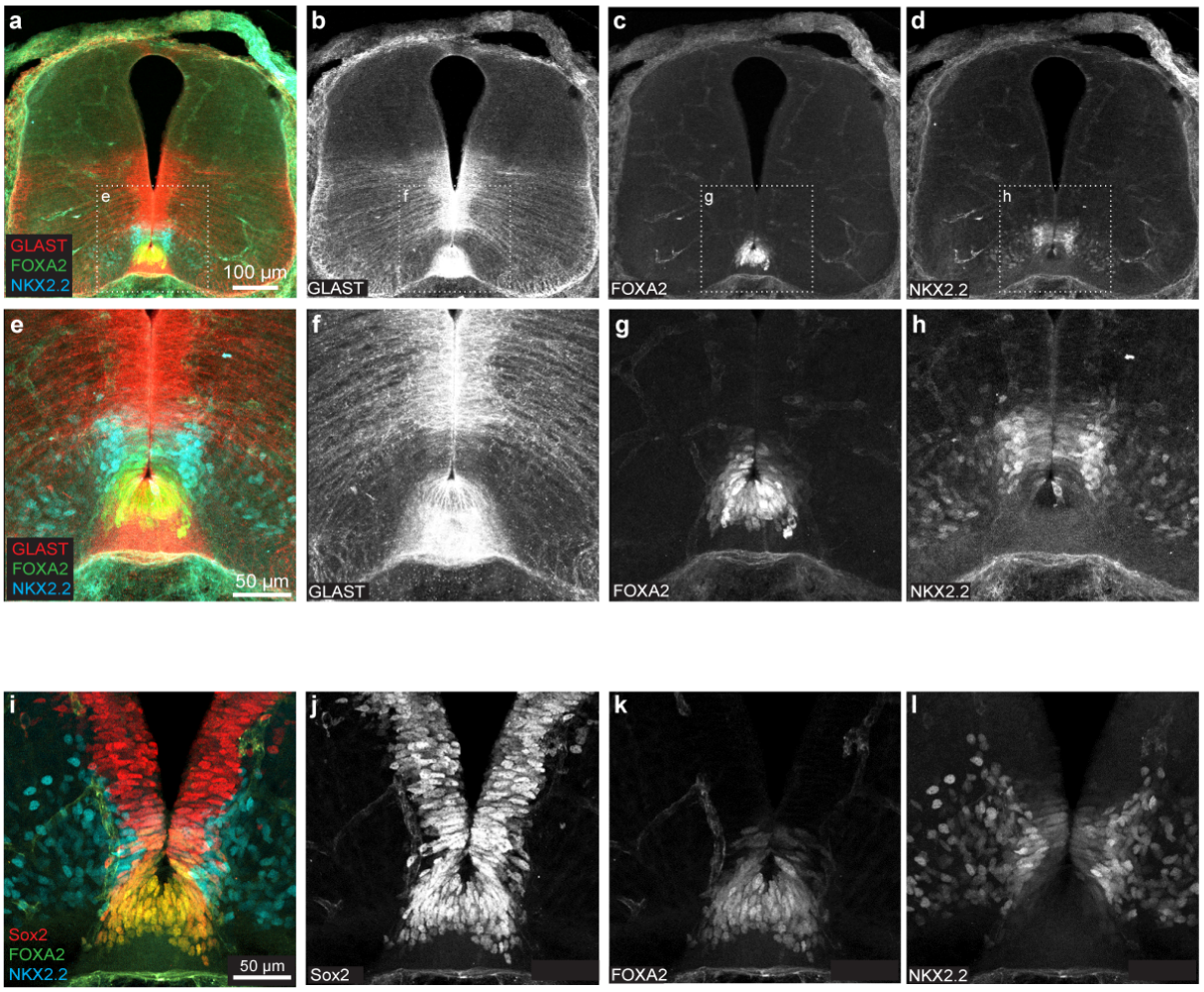

Extended Data Figure 1. Floor plate cells co-express GLAST, a marker of glial progenitors, and Sox2, a marker of neuro-epithelial progenitors

a-d, Confocal images showing the expression of the glial marker GLAST (red in a, greyscale in b), the floor plate marker FoxA2 (green in a, greyscale in c) and the p3 domain marker Nkx2.2 (cyan in a, greyscale in d) in a coronal section of a E12.5 mouse embryonic spinal cord. **e-h** Higher magnification confocal image of the same coronal section shown in a-d (dotted area). Note that $FoxA2^{+}/NKX2.2^{-}$ cells located in the floor plate co-expressed the glutamate astrocyte transporter GLAST. **i-l,** confocal image showing the expression of the neuro-epithelial marker Sox2 (red in i, greyscale in j), the floor plate marker FoxA2 (green in i, greyscale in k) and the p3 domain marker Nkx2.2 (cyan in i, greyscale in l) in a coronal section of a E12.5 mouse embryonic spinal cord. Note that all $FoxA2^{+}/NKX2.2^{-}$ cells located in the floor plate co-expressed Sox2.

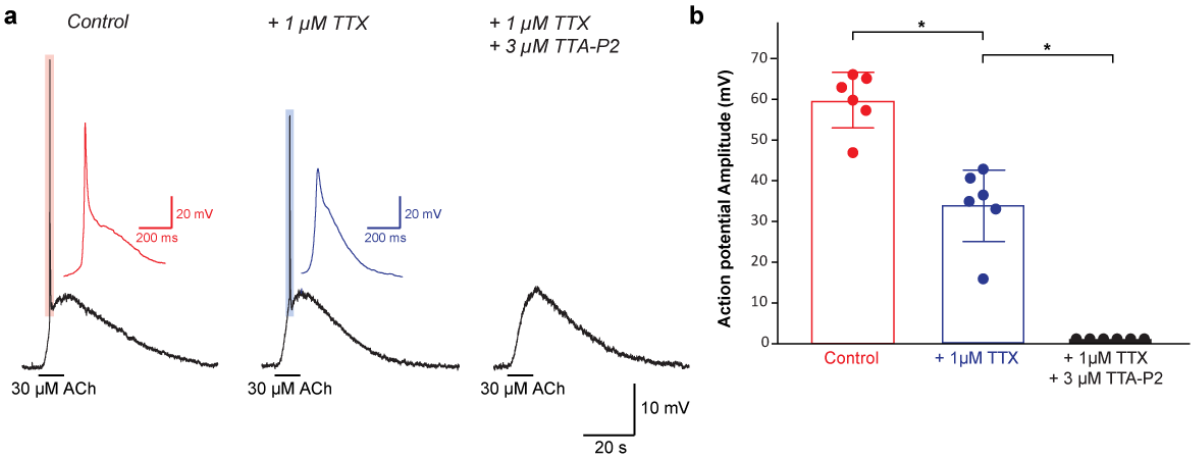

Extended Data Figure 2. Floor plate action potentials evoked by acetylcholine rely on both TTX-sensitive voltage-gated sodium channels and T-type voltage-gated calcium channels.

a, Example of current-clamp recording showing a biphasic floor plate action potential evoked by the application of acetylcholine (30 μM, left trace), after application of the voltage-gated sodium channel blocker TTX (1μM, middle trace) and after the subsequent addition of the T-type voltage-gated calcium channel blocker TTA-P2 (3 μM, right trace). Note that the fast component of the action potential was blocked by TTX while the slow component was only blocked after addition of TTA-P2. **b**, Plot quantifying the effect of TTX and TTA-P2 on the amplitude of floor plate action potential evoked by acetylcholine.

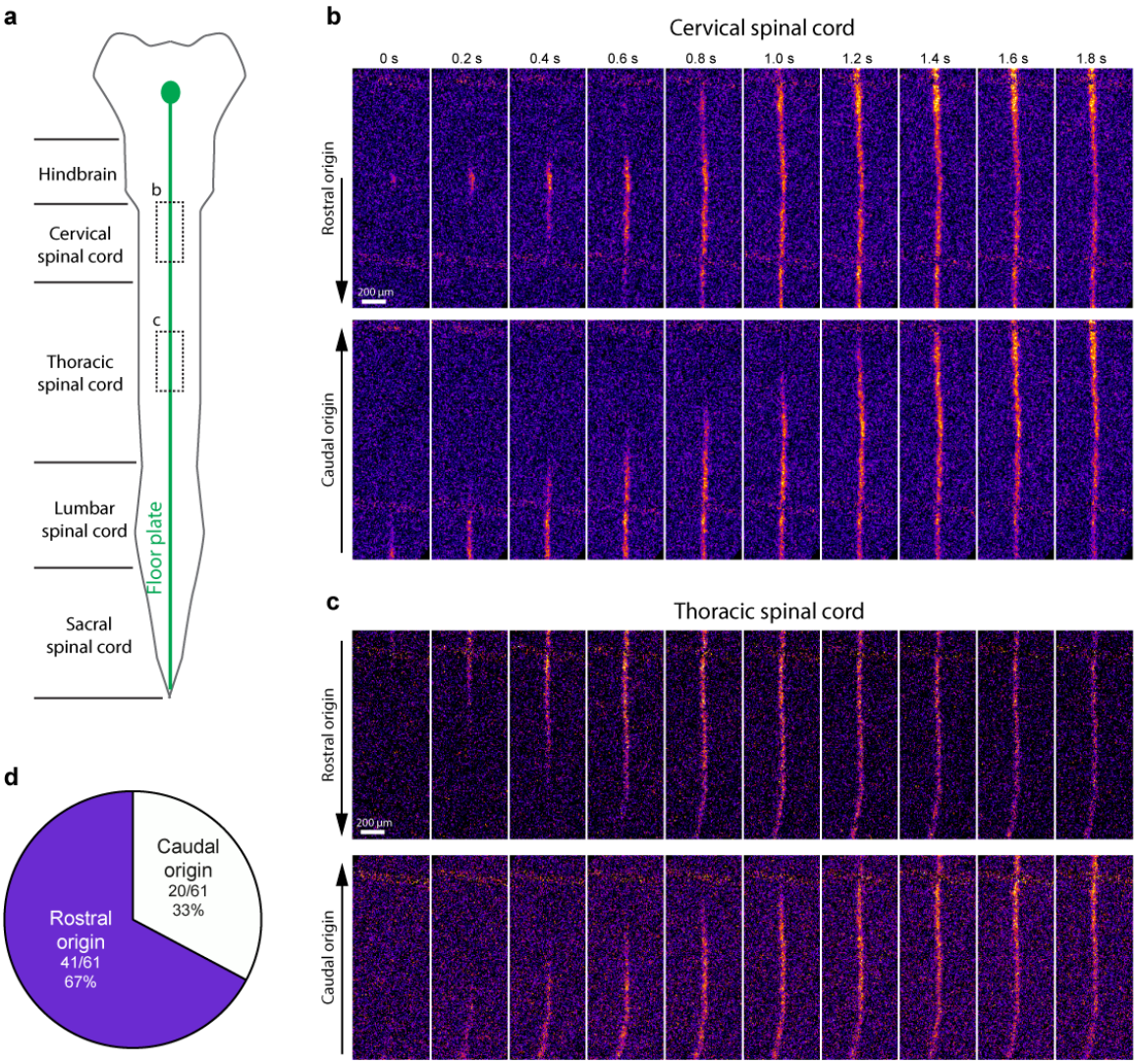

Extended Data Figure 3. Spontaneous calcium waves in the floorplate can propagate in both directions and originate from rostral or caudal locations.
a, Drawing representing a longitudinal view of an open-book preparation of the spinal cord at E12.5. The floor plate is represented in green. **b**, Time lapse images showing the evolution of GCaMP6 fluorescent signal in the floor plate at the cervical level using an open-book preparation of spinal cord from a E12.5 transgenic mouse embryo (GLAST:CreERT2 x floxed-GCaMP6f). Examples of spontaneous floor plate calcium waves with a rostral origin (top panel) and caudal origin (bottom panel) are shown. In the top traces, the wave originated from the cervical area and propagated in both directions. **c**, Time lapse images showing the evolution of GCaMP6 fluorescent signal in the floor plate at the thoracic level. An example of each type of wave is shown (top panel: rostral origin, bottom panel: caudal origin). **d**, Proportion of spontaneous calcium wave originating respectively from a rostral and caudal origin in both regions (N = 61 waves; 10 embryos).

EXTENDED DATA VIDEOS

Extended Data Video 1. Example of background subtraction performed on a spontaneous calcium wave recorded at thoracic level.
Left, Raw time-lapse recording (10 Hz) of GCaMP6 fluorescent signal showing a spontaneous floor plate calcium wave recorded at thoracic level using an open-book preparation of spinal cord from a E12.5 transgenic mouse embryo (GLAST:CreERT2 x floxed- GCaMP6). Right, The same time-lapse recording (10 Hz) after subtraction of background GCaMP6 fluorescence.

Extended Data Video 2. Spontaneous floor plate calcium waves can propagate in either direction.
Time lapse movies (10 Hz, background subtraction) showing two examples of floor plate calcium waves recorded at thoracic level in the same open-book preparation exhibiting either a rostral (left movie) or a caudal origin (right movie).

Extended Data Video 3. Evoked floor plate calcium waves are consistently triggered by consecutive electrical stimulation.
Time lapse movies (10 Hz, background subtraction) showing 3 consecutive floor plate calcium waves recorded at thoracic level in response to electrical stimulation (32 mA/200 µs) located in the cervical area.

Extended Data Video 4. Evoked floor plate calcium waves are completely blocked by the T-type calcium blocker TTA-P2.
Time lapse movies (10 Hz, background subtraction) showing examples of a calcium wave evoked in control condition (left movie; 32 mA/200 µs), after addition of TTA-P2 (middle movie; 32 mA/200 µs) and after subsequent increase of stimulation duration (right movie; 32 mA/1200 µs). Note that the T-type calcium channel blocker TTA-P2 (3 µM) completely blocked the floor plate calcium wave, which is not restored after increasing the duration of electrical stimulation.

Extended Data Video 5. Evoked floor plate calcium wave propagation depends both on nAChR and gap-junction coupling.
Time lapse movies (10 Hz, background subtraction) showing examples of a calcium wave evoked in control condition (first movie; 32 mA/200 µs), after addition of nAChR antagonist (second movie; 32 mA/200 µs), after subsequent increase of stimulation intensity (third movie; 32 mA/1200 µs) and after final addition of the gap-junction blocker β18-GA (fourth movie). Note that the floor plate calcium wave propagation was partially restored by increasing the intensity of electrical stimulation and that it was subsequently reduced by addition of gap junction blocker.